University of California
Ernest O. Lawrence
Radiation Laboratory

LAPARK-CHAMBER PULSE MODULATORS

Berkeley, California

DISCLAIMER

For Wescon - IEEE - San Francisco, Aug. 20-23, 1963 UCRL-10887

UNIVERSITY OF CALIFORNIA
Lawrence Radiation Laboratory
Berkeley, California

Contract No. W-7405-eng-48

SPARK-CHAMBER PULSE MODULATORS

Quentin A. Kerns

June 1963

SPARK-CHAMBER PULSE MODULATORS

Quentin A. Kerns
Lawrence Radiation Laboratory
University of California
Berkeley, California

Summary: Spark chambers are widely used in high-energy nuclear physics to display the trajectories of ionizing particles. There is no doubt that the spark chamber will continue to be a powerful tool for the study of nuclear events with the ultrahigh-energy particle accelerators of the future. [1] The techniques of generating the high-power electrical pulses for spark-chamber operation are discussed in this report. In order to clarify the requirements that must be met by a spark-chamber pulse modulator, the typical operation and timing of a spark chamber system is described, together with the features of chamber operation and construction that affect modulator design. An important aspect of system operation is the time delay through various stages of the modulator; values are given for a trigger amplifier which precedes the modulator. Existing modulator designs and power figures are discussed, with emphasis on the triggered gap as a modulator switching element. A developmental electron-triggered gap is described which can significantly reduce time delay, rise time, and jitter.

I. Spark Chamber

Typical Operation

Figure 1 illustrates an application of the spark chamber. The incident particle enters from the left, passes through the scintillation counters, and interacts in the liquid hydrogen target. The final-state particle emerges from the target and passes through the spark chamber, leaving a trail of ions in the spark-chamber filling gas (~ 10-30 ion pairs/cm path length for minimum-ionizing particles and 1 atm. chamber pressure). Passage of the particle is detected by the scintillation counters. If suitably related signals (the signature of the desired event) appear at the coincidence circuit, a trigger pulse is generated and fed to the modulator. The pulse modulator in turn drives the spark-chamber plates with a high-voltage pulse, causing the ion trail to develop into a visible spark between plates. Strobe lamps are simultaneously flashed to illuminate fiducial lines which are recorded by the camera along with the spark.

Timing Sequence

Figure 2 illustrates the spark-chamber timing sequence, and Table I lists representative values of the time intervals. After the particle passes (line A of Fig. 2), the chamber remains sensitive for a period $t_5 - t_0$. The deflector signals (line C) must appear at the coincidence-anticoincidence circuit with little delay in order that the decision to fire or not fire the chamber occur within the chamber sensitive time.

Information Readout

Photographic or television cameras are employed in spark-chamber viewing, which is normally done stereoscopically (with mirrors) to allow reconstruction of the tracks in space. Sometimes transparent plates are used to construct a "face view" chamber. Other means of reading out the position of a spark include timed detection of the acoustic shock wave from the spark[2] and use of wire arrays in the chamber feeding magnetic memory cores[3] or magnetic tape.[4]

Plates

The plates may be made of any electrical conductor (semiconductors such as glass have also been used).[5] Carbon plates have been used for proton scattering. Thin-plate chambers are used to measure particle direction with minimum scattering,[6] and have been made with foils as thin as 7 μ.[7] On the other hand, the large neutrino chambers,[8,9] may contain 10 to 25 tons of material in the form of aluminum or brass plates. Various workers have coated the plates with insulating or semiconducting films to limit the current of any single spark, although one can observe several sparks/gap without coating.[10] Cylindrical chambers surrounding a target afford a large solid angle of detection.[9,11]

Gap Distance: The Discharge Chamber

Gap distance (spacing between plates) can be as small as a millimeter or as large as several centimeters. Small gaps will have fewer ion pairs per gap, and therefore may not always fire after particle passage, i.e., the detection efficiency may not be 100%. The limit on large gaps is one of spacial resolution: since the sparks tend to develop along the direction of the electric field, the particle trajectory is well defined in two dimensions (to a fraction of 1 mm), but limited to the gap distance in the third. There is another class of spark chamber, the discharge chamber, which employs a wide gap and appears to produce a well-defined track in three dimensions. The discharge chamber is presently being explored at Berkeley and elsewhere.[5,12,13] In such a chamber, particle identification by ionization density,[14,15] may be quite feasible. A discharge can be developed by application of microwave energy.[16-18] Microwave excitation of a wide-gap chamber would permit viewing the tracks of particles that traverse the chamber parallel to the plates.

Magnetic Fields

To obtain momentum and sign information, one can observe the particle direction by using spark chambers at the entrance and exit of the analyzing magnet or the chamber itself may be immersed in a magnetic field.[19-23, 13] The latter arrangement gives curved tracks, with

$$\rho = \frac{P}{Be} \qquad (1)$$

where ρ is the radius of curvature, B is the magnetic induction, P is the particle momentum, and e is the electronic charge.

Sensitive Time

Since many particles traverse the chamber, whereas relatively few are selected as "interesting" by the coincidence-anticoincidence logic, the old ion trails must be swept from the gases used for chamber filling. Electrical clearing fields of 10 to 1000 volts/cm sweep out ions and thus reduce the sensitive time $t_5 - t_0$. If sufficient clearing field is applied, the chamber sensitive time can be made small enough to allow triggering on single events in a particle flux as great as 10^6/sec. Alternatively, electron-attaching gases have been added (e.g., 1/4% SO_2 in Ne) to reduce the sensitive time, thus avoiding a clearing field.[20, 24]

II. Trigger Amplifier

The event trigger pulse of about 1 volt amplitude from the coincidence circuit (Fig. 1) must be amplified to a level sufficient to drive the pulse modulator. Figure 3 shows the simplified schematic of a trigger amplifier of four stages, all normally nonconducting. Following are the essential properties of the amplifier:

Repetition rate	0 to 50 pps
Input impedance	50 ohms
Output impedance (2 parallel 50Ω)	25 ohms
Input-pulse level	1 volt
Input-pulse length	1 to 10 nsec
Output-pulse level	10,000 volts
Output-pulse length	25 nsec
Output-pulse rise time	10 nsec
Power gain	83 db
Delay time	32 nsec
Shielding factor against stray radiation	> 100 db

The individual stages contribute to the power gain and delay as shown in Table II.

The avalanche transistor stage uses selected transistors.[25] A corona lamp is essential to the operation of the triggered gap stage.[26]

The trigger amplifier is considered as simply a building block to raise the signal level from 1 volt to 10 kV at the 50-ohm impedance level, and has been used with a number of pulse modulators.

III. The Pulse Modulator

Figure 4 represents a pulse modulator for a multigap chamber. The energy-storage capacitor C_A is commonly several times the chamber and wiring capacitance C_C. A voltage pulse is produced at C_C by firing the triggered gap S, which may be one of the types shown in Figs. 5, 6, and 7. (The high-voltage pulse should have a rapid rise. If the pulse rises slowly, previously-deposited electrons will be swept out by the rising pulse front, preventing the formation of a discharge when the avalanche voltage is attained. Efficient operation of a chamber with gaps of a few millimeters requires rise times, τ_1, of 10 nsec or less). In Fig. 4 L_p and R_p represent the stray resistance and inductance of the switch and wiring. The buildup of current in switch S is not instantaneous, and therefore complicates the calculation of the waveshape at C_C, as do the charge oscillations that occur but are not shown in the waveform of Fig. 4. Since development of the chamber discharge takes place either with unidirectional pulses or a damped wave, pulses usually are not elaborately shaped. An exception is the matched impedance system, which is discussed later. The decay τ_2 is the discharge time constant of $(C_A + C_C)R$ in the event a gap fails to fire, and is typically made 100 to 300 nsec. A simple exponential decay is most common, although flat-topped pulses have been employed for special purposes, generated usually by line-type pulsers.

Electric-Field Requirements

The main function of the modulator is to provide a pulsed electric field within the spark-chamber volume. To estimate modulator power, consider the magnitude of the typical field, given in Table III. With these values of E, a single electron in the gap will avalanche and result in a spark after the spark-formation time $t_4 - t_3 = \Delta t$. The spark formation time depends upon E as follows: For $\Delta t > 20$ nsec, we have

$$\Delta t = ae^{-bE} \text{ sec}, \qquad (2)$$

where

$a = 1 \times 10^{-6}$ for argon
$= 1.0 \times 10^{-7}$ for 90% Ne-10% He.
$b = 1.68 \times 10^{-4}$ for argon
$= 1.84 \times 10^{-4}$ for 90% Ne-10% He.

A practical lower limit for E is $\approx 4 \times 10^5$ V/meter in 90% neon - 10% helium, and 8×10^5 V/meter in argon.

Power Calculation for Lumped Constant System:

Let:
U_C = electrostatic energy in chamber, joules
U_A = electrostatic energy in storage capacitor, joules
E = electric field in chamber, volts/meter
ϵ_0 = permittivity of free space = 8.85×10^{-12} F/meter

μ_0 = permeability of free space = $4\pi \times 10^{-7}$ h/meter
ϵ = permittivity of chamber gas ≈ 1
c = velocity of light in free space
v = active volume of chamber = gLW × number of gaps
C_A = storage capacitance
C_C = chamber capacitance
V = peak pulse voltage
P_U = power pulse associated with charging of C_C
P_R = peak power dissipated in R
g = gap spacing, meters
W = plate width, meters
L = plate length, meters

The pulse modulator transfers energy from C_A to C_C during τ_1, and maintains voltage across R during the pulse. (Here we assume that the rise time τ_1 is greater than the signal transit time L/c through the chamber. For $\tau_1 \leq L/c$, we must calculate power as for the impedance-matched system.)

It is interesting to compute P_U and P_R:

$$P_U = \frac{d}{dt}\,(U_C),$$

where

$$U_C = \frac{\epsilon\epsilon_0}{2} \int E^2\, dv = 4.5 \text{ joules/meter}^3$$

if

$$E = 10^6 \text{ V/meter.}$$

Assuming linear charging of C_C for estimating P_U, we have

$$P_U = \frac{\frac{\epsilon\epsilon_0}{2} \int E^2\, dv}{\tau_1}.$$

Examples: P_U ≈ 100 MW for a 1-meter^3 chamber with 45-nsec rise time:
≈ 200 kW for a 100-cm^3 chamber with 22-nsec rise time.

It is useful to obtain an estimate of P_R in terms of τ_2. Let $C_A = 4\,C_C$ (typical) and assume that the charge initially on C_A is shared by $C_A + C_C$ after switching. Then an energy $U_A/5$ is lost in the switching operation, leaving an energy $4U_A/5 = 5\,U_C$ to be absorbed by R. Thus we have

$$P_R = \frac{d}{dt}\,(5\,U_C) = \frac{5U_C}{\tau_2}.$$

For $\tau_2 = 10\,\tau_1$, we have

$$P_R = \frac{5\,U_C}{10\,\tau_1} = P_U/2.$$

Power Calculation for Matched Impedance Systems

An upper limit for the required pulse modulator power can be deduced by calculating the Poynting vector $\vec{N} = \vec{E} \times \vec{H}$ at the spark-chamber entrance where energy is introduced. One assumes that the energy is delivered as a plane-polarized wave, with $\vec{E}$ directed across the spark chamber gap, whence we have

$$\frac{\text{peak power}}{\text{unit area}} = N = \sqrt{\frac{\epsilon_0}{\mu_0}}\,E^2 = \frac{E^2}{377} \text{ watts/meter}^2.$$

Alternatively, one can assume a matched-impedance line-type pulse modulator to be employed, and consider the spark chamber to be a short length of parallel-plate transmission line. The characteristic impedance Z_0 of the spark chamber depends upon the plate width and spacing. The spark chamber (if it has many gaps) is considered as a number of 2-plate modules, or of 3-plate modules having the center plate energized and the two outer plates grounded. If we neglect edge effects, the 3-plate module is a parallel combination of a pair of 2-plate modules. Then we have

$$\text{peak power} = \frac{V^2}{Z_0}.$$

A parallel-plate chamber has a characteristic impedance:

$$Z_0 = \sqrt{\frac{\mu_0}{\epsilon_0}}\,\frac{g}{W} \text{ ohms.}$$

Since we have V = gE, we obtain:

$$\text{peak power} = \frac{V^2}{Z_0} = \frac{g^2E^2}{\sqrt{\frac{\mu_0}{\epsilon_0}}\,\frac{g}{W}} = \frac{WgE^2}{377}.$$

Since Wg represents the cross-sectional area at the spark-chamber entrance where energy is delivered, we find, as before,

$$N = \frac{\text{peak power}}{Wg} = \frac{E^2}{377} \text{ Watts/meter}^2.$$

Taking $E = 10^6$ V/meter, we find

$$N = \frac{E^2}{377} = \frac{10^{12}}{377} = 2{,}650 \text{ MW/meter}^2.$$

If we wish to avoid reflections in the matched system, the chamber plates must be terminated in a distributed resistance equal to Z_0 to absorb the power. If we assume that a flat-topped pulse of length τ is used, the energy absorbed is $E^2\tau/377$ joules per meter^2; τ must be longer than the spark formation time, Δt. For τ = 50 nsec, the energy per pulse is 133 joules per meter^2. One should remember that the electric field is applied to the chamber to make it spark, and when it does, the impedance of the system is suddenly no longer matched. (The waves set up by the spark could, in principle, be used to locate its position, but the timing accuracy would have to be better than that of the sonic chamber

by the ratio of light velocity to acoustic-shock-wave velocity.)

Unless the chamber is small, the power required in an impedance-matched system is discouragingly large. The foregoing accounts for the popularity of the lumped systems such as that illustrated in Fig. 4, where the electric field rises in a series of steps corresponding to the electrical reflections from the open-circuited spark-chamber plates.

Even with the lumped circuit, it is usual to share the total power among several modulating gaps, and use an individual capacitor C_A and a separate connecting cable (L_P) to each spark-chamber gap or pair of gaps. Figure 8 illustrates such an energy-distribution system. It is connected to the spark chambers shown in Figs. 9 and 10. Table IV shows the constants of the pulse modulator system of Figs. 8 to 10.

Figure 11 shows the wide-gap chamber whose constants are given in Table V. The modulator has been used to produce tracks in a Linde rare-gas flask containing pure neon at 1 atm. pressure. The plates of the spark chamber were outside the spherical glass (1-liter) flask. Figure 11 shows a cosmic-ray muon traversing a chamber constructed of parallel aluminum plates and Lucite walls. The filling gas is 90% Ne - 10% He. The voltage pulse has the shape shown in Fig. 4, with τ_1 = 20 nsec, τ_2 = 200 nsec, and V = 140 kV.

IV. Triggered Gap Development

Figure 5 shows the arrangement of an air spark gap triggered by a corona lamp. The spark-chamber energy-distribution box, Fig. 8, contains two such gaps. It is worth noting that no sharp points are used in the gap. Erosion problems are thus avoided.

Figure 6 shows a version of corona-lamp triggered gap with lamp and electrodes enclosed in a pressure chamber of 50-ohm coaxial geometry. Lamp effectiveness is improved by the use of an ellipsoidal reflector.

The gap operation may be considered in four stages. In stage 1, the electrode 1 potential is pulsed 10 kV negative in a few nanoseconds, raising the electric field between electrodes 1 and 2 to a level where a single injected electron will lead to an avalanche. In stage 2, the corona lamp is fired, ejecting precisely-timed photoelectrons from electrode 1, which multiply exponentially in the 1-2 gap. In stage 3, electrode 1 (which has become positive with respect to electrode 3) develops an electron avalanche to electrode 3. During stage 4, the resistivity of the 1-2 and 1-3 gaps falls with time to a value of ~ 10^{-3} ohms-cm.

Photoelectron currents of ~ 10 μa at gap electrode 1 can be generated with the lamp- and-mirror combination.

At a pressure of 3 to 4 atm N_2, the rise time is ~ 0.5 nsec. The jitter has been measured to be < 1 nsec at 7 kV output (~ 1 MW). Similar gaps have been used at power levels up to 40 MW, with an increase in rise time to ~ 5 nsec.

Figure 7 shows a switch tube being developed to reduce rise time, delay, and time jitter of high-power gaps. A thermionic trigger tube provided with a thin vacuum-tight window allows electrons to penetrate the pressurized gap atmosphere. The gap electrodes are perforated with parallel channels to allow entry of electrons and to separate the thin window from the discharge region. This design eliminates the trigger amplifier of Fig. 3. One can estimate that the delay time between receipt of a 1-V pulse at the avalanche transistor input of the electron-triggered pressurized switch and the 50% amplitude point on the leading edge of the output pulse will be < 5 nsec, with sub-nanosecond jitter and rise time. With this switch, very short sensitive times become practical for a spark chamber, allowing single-event selection at very high particle rates. Low jitter time permits the parallel operation of many gaps to produce a higher-power pulse while retaining a steep leading edge.

V. Conclusions

The spark-chamber art has developed rapidly, and a wide variety of pulse modulators has been used to power pulsed chambers that can range in size from 10 cm^3 units to be flown in satellites, up to massive chambers of several $meters^3$ volume. Pulse modulator power depends on the desired electric field (~ 10^6 V/meter), the chamber volume WLg, and the desired rise time of the voltage pulse. Matched-impedance systems are necessary to attain the ultimate in fast rise time, but require a maximum modulator peak power.

It appears that development of large radio-frequency and microwave chambers has been delayed by the lack of fast-rising multi-megawatt radiofrequency power sources. As possible solutions to the radiofrequency power problem, in addition to magnetrons which have been used,[16] one should consider (a) high-power traveling-wave tubes (rise times of 1 to 2 nsec are possible) and (b) resonator storage of radiofrequency energy,[28, 29] with subsequent transfer to the load via a fast-acting switch.

Acknowledgments

It is a pleasure to acknowledge the advice and support of the Physics Research groups of the Lawrence Radiation Laboratory, for whom this work is being done. Particular thanks is due Dr. Victor Perez-Mendez, part of whose experimental set-up is shown in Figs. 9 and 10, and Dr. Kenneth Crowe, whose group is studying the gas-discharge phenomena of the wide-gap chamber of Fig. 11. This work was supported by the U. S. Atomic Energy Commission.

References

1. J. Sandweiss, "Experimental Techniques at Ultra-High Energies," Nucl. Instr. Methods 20, 1 (1963).

2. B. C. Maglić, "The Sonic Spark Chamber and Some of its Experimental Aspects," Nucl. Instr. Methods 20, 165 (1963).

3. F. Kreinen, "A Digitized Spark Chamber," Nucl. Instr. Methods 20, 168 (1963).

4. M. J. Neumann and H. Sherrard, "Spark Chamber for Electronic Data Retrieval," IRE Trans. Nucl. Sci. NS-9, 259 (June, 1962).

5. G. Peter, A. A. Tyapkin, A. F. Pisarev, and Tzou Chu-Lyang, "The Appearance of Inclined Discharge Channels Along An Ionizing Particle Track," Nucl. Instr. Methods 20, 201 (1963).

6. E. Bleuler, D. O. Caldwell, B. Elsner, D. Harting, L. W. Jones, W. C. Middelkoop, B. Zacharov, M. L. Perl, and C. C. Ting, "The Application of Thin-plate Spark Chambers to High-Energy π-p Experiments," Nucl. Instr. Methods 20, 208 (1963).

7. Yu. D. Bayukov, G. A. Leksin, D. A. Suchkov, and V. V. Telenkov, "Spark Chambers With Small Amount of Material Along the Tracks, Nucl. Instr. Methods 20, 198 (1963).

8. H. Faissner, F. Ferrero, A. Ghani, E. Heer, F. Krienen, G. Muratori, T. B. Novey, M. Reinharz, and R. A. Salmeron, "The CERN Neutrino Spark Chamber," Nucl. Instr. Meth. 20, 213 (1963).

9. J. W. Cronin, "Spark Chambers - State of the Art," IRE Trans. Nucl. Sci. NS9, No. 3, 247 (1962).

10. H. Faissner, F. Ferrero, A. Ghani, F. Krienen, T. B. Novey, and M. Reinharz, "Spark Chamber Efficiency for Electron Shower Detection," Nucl. Instr. and Meth. 20, 161 (1963).

11. E. F. Beall, W. Holley, D. Keef, L. T. Kerth, J. J. Thresher, C. L. Wang, and W. A. Wenzel, "Cylindrical Spark-Chamber Array Used for the Measurement of Angle, Range, and Polarization in a Study of K^--p Interactions," Nucl. Instr. Methods 20, 205 (1963).

12. A. A. Tyapkin, "The Appearance of a Discharge in a Flat Controlled Counter Along a Particle Track," in Proceedings of an International Conference on Instrumentation for High-Energy Physics (Lawrence Radiation Laboratory, Berkeley, California, 1960), p. 270.

13. A. I. Alikhanian, T. L. Asatiani, A. M. Matevosian, and R. O. Sharkhatunian, "Momentum Measurements of Charged Particles in a Single Gap Spark Chamber Placed in Magnetic Field," Phys. Letters 4, 295 (1963).

14. E. Engels, D. Roth, J. Cronin, and M. Pyka, "Ionization Density Effects in Spark Chambers," IRE Trans. Nucl. Sci. NS-9, No. 3, 256 (1962).

15. C. T. Coffin, L. J. Curtis, D. F. Meyer, and K. M. Terwillinger, "Use of Relative Ionization for Particle Identification in Multitrack Spark Chamber Pictures," Nucl. Instr. Methods 20, 156 (1963).

16. S. Fuki, S. Hayakawa, T. Tsukishima, and H. Nukushina, "Microwave Discharge Chamber," Nucl. Instr. Methods 20, 236 (1963).

17. C. Cavalleri, E. Gatti, and G. Redaelli, "Light Chamber or Gas Amplified Scintillation Chamber," Nucl. Instr. Methods 20, 238 (1963).

18. S. Fukui, S. Hayakawa, T. Tsukishima, and H. Nukushina, "The Microwave Discharge Chamber -- A New Type of Particle Detector," in Proceedings of an International Conference on Instrumentation for High-Energy Physics (Lawrence Radiation Laboratory, Berkeley, California, 1960), p. 267.

19. D. Keefe, L. T. Kerth, C. M. Noble, J. J. Thresher, and W. A. Wenzel, "A Magnetic Spectrometer Using Spark Chambers to Obtain Large Solid Angle and High Resolution in π-π Interaction Studies," Nucl. Instr. Methods 20, 171 (1963).

20. G. K. O'Neill, F. V. Murphy, K. Wright, and D. Yount, "Magnetic-field Spark Chambers," Nucl. Instr. Methods 20, 176 (1963).

21. G. R. Burleson, T. F. Hoang, P. I. P. Kalmus R. L. Kuskowshi, L. Q. Niemela, A. Roberts, T. A. Romanowski, S. D. Warshaw, and G. E. Yurka, "Design and Construction of a Large Magnetic-Field Spark Chamber System," Nucl. Instr. Methods 20, 180 (1963).

22. G. R. Burleson, T. F. Hoang, P. I. P. Kalmus, R. L. Kuskowshi, L. Q. Niemela, A. Roberts, T. A. Romanowski, S. D. Warshaw, and G. E. Yurka, "Initial Operation and Performance of a Large Magnetic-Field Spark Chamber System," Nucl. Instr. Methods 20, 185 (1963).

23. K. Lande, A. K. Mann and D. H. White, "A Simple Optical System for Using Standard Magnets with Spark Chambers," Nucl. Instr. Methods 20, 193 (1963).

24. F. Schneider and K. H. Hohne, "Influence of Gas Admixtures on the Sensitive Time of Spark Chambers," Nucl. Instr. Methods 20, 152 (1963).

25. Harold W. Miller and Quentin A. Kerns, "Transistors for Avalanche-Mode Operation," Rev. Sci. Instr. 33, 877 (1962).

26. Thomas G. Innes and Quentin A. Kerns, "A Pulsed Nanosecond Light Source," Western Electronic Show and Convention Record, August 22-25, 1961.

27. Joachim Fischer and Gus T. Zorn, "Reduction of Delay Between Particle Passage and Spark-Chamber Spark, IRE Trans. Nucl. Sci. NS-9, 261 (1962).

28. S. J. Miller, "The Traveling-Wave Resonator and High Power Testing," Microwave J. 3, 50 (1960).

29. D. B. Schwarzkopf, "The Traveling-Wave Resonator as a Short Pulse Generator," Microwave J. 5, 172 (1962).

Table I. Timing intervals in spark-chamber operation

Interval	Time	Remarks
$t_1 - t_0$	5 - 80 nsec	Minature phototubes operated at high voltage/stage reduce $t_1 - t_0$.
$t_2 - t_1$	2 - 20 nsec	Tunnel diode logic is useful for achieving short delay.
$t_3 - t_2$	15 - 500 nsec	Combined delay of trigger and pulse modulator is quoted.
$t_4 - t_3$	10 - 100 nsec	Let $t_4 - t_3 = \Delta t$. Then Δt^{-1} varies exponentially with the chamber field E.
$t_5 - t_0$	0.1 - 20 μsec	The chamber is sensitive until t_5 unless chamber is pulsed, in which case chamber sensitivity ceases at t_4.
$t_8 - t_4$	10 - 100 msec	Mechanical cameras can recycle in ~40 msec Television cameras may scan in ~10 msec. Other readout means may be more rapid.
$t_7 - t_4$	5 - 60 msec	Ions are collected and metastable atoms decay in this time.
$t_6 - t_5$	1 - 20 msec	An electrical clearing field can sometimes be avoided through the use of electronegative scavenging gases (chemical clearing).

Table II
Stage gain and delay of trigger amplifier

Stage	Voltage level (volts)	Current level (amperes)	Power gain (db)	Delay time (nsec)
Avalanche transistor (TR1 - TR2)	[redacted]	[redacted]	[redacted]	[redacted]
	100	1	37	3
Microwave triode (7815)	600	2	11	5
Microwave triode (ML-DP30)	8,000	10	18	7
Triggered gap	10,000	400	17	17
		Totals:	83	32

Table III
Typical electric field for spark formation

Gas	Ne + 0 5% A	10% He + 90% Ne	He
Pressure, atm	1.5	1	1
E, MV/meter	0.6	1	1 - 1.3
Gas	A	Ne	A - 0_2
Pressure, atm	1	1	1
E, MV/meter	1.2	0.5	1.6

Table IV
System parameters for the 2-MW pulse modulator and spark chambers of Figs. 9 and 10

Chamber designation	Module type	No. of gaps	Dimensions and capacitance[a] W (in.)	L (in.)	g (in.) C (pF)	L_p[a,b] (ft)	C_A[a] (pF)	R[a] (ohms)
Entrance to bending magnet	4 each, 3 plate modules; 1 high-voltage plate/mod.	8	6	12 105	5/16	6	2000	88
Exit of bending magnet 2 each	7 plates: 3 high-voltage plates, 4 common plates	6	15	36 780	5/16	10	4000	88
Target size A 2 each	7 plates: 3 high-voltage plates, 4 common plates	6	24	24 690	3/8	10	4000	88
Target size B 2 each	7 plates: 3 high-voltage plates, 4 common plates	6	27	35 1130	3/8	10	4000	88

[a] Values given are per high-voltage plate.

[b] Length in feet of RG/9U cable.

Table V
System parameters for the 100-MW pulse modulator and wide-gap discharge chamber of Fig. 11

Type of chamber	Dimensions	C_C (pF)	C_A	L_P (μH)	R (ohms)
2-plate, wide gap	W = 18 in. L = 24 in. g = 20 cm	40-50	1000 pF at 140 kV	0.8	200

Figure Legends

Fig. 1. Spark-chamber triggering and viewing arrangement.

Fig. 2. Spark-chamber timing sequence.

Fig. 3. Trigger amplifier.

Fig. 4. Pulse modulator circuit.

Fig. 5. Air spark-gap triggered by corona lamp.

Fig. 6. Pressurized ultraviolet-triggered switch.

Fig. 7. Electron-triggered pressurized switch.

Fig. 8. Spark-chamber energy-distribution box.

Fig. 9. View of target area in inelastic pion-nucleon interaction experiment.

Fig. 10. Spark chambers and analyzing magnet for study of inelastic pion-nucleon interactions.

Fig. 11. Wide-gap discharge chamber.

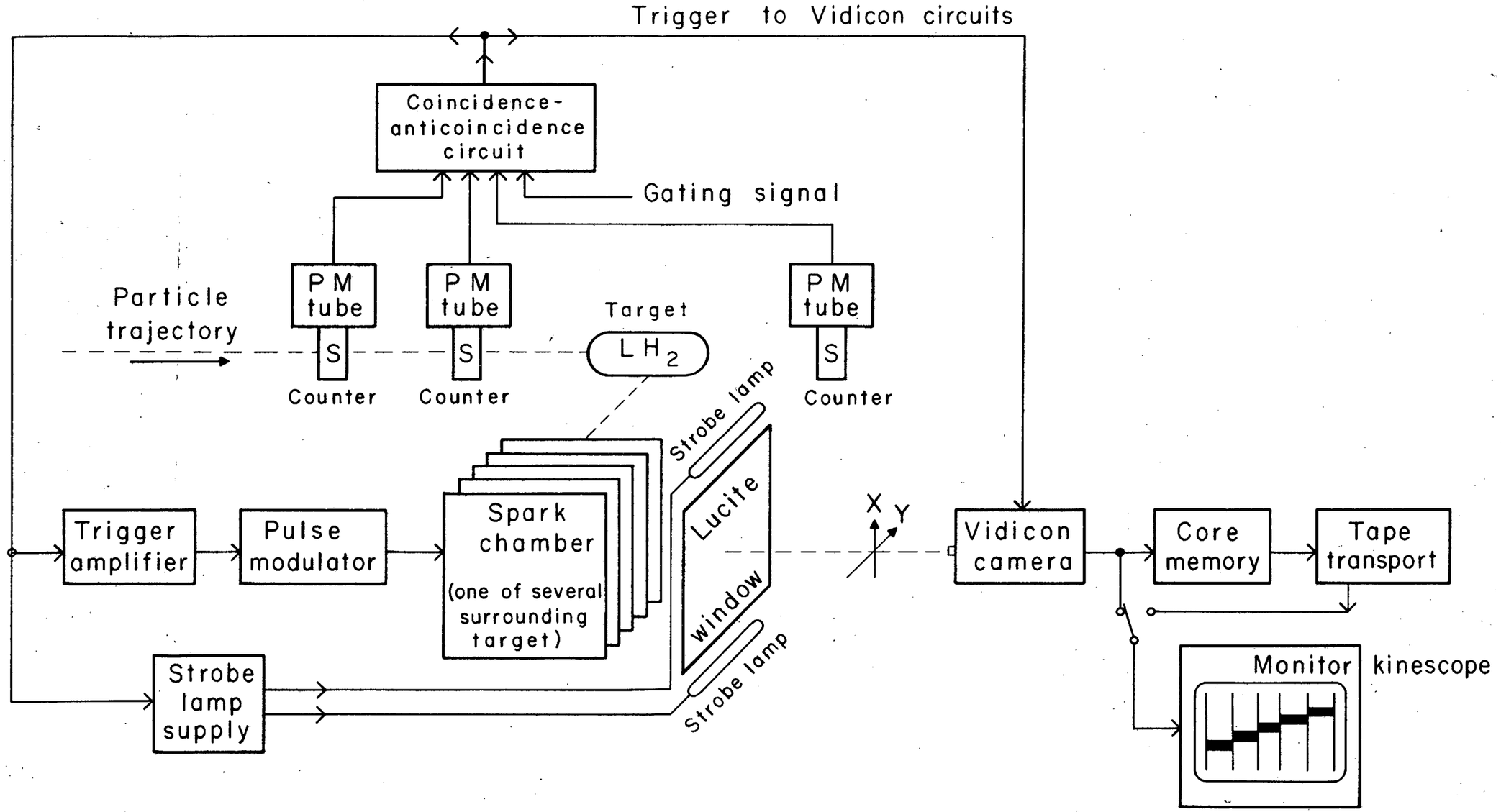
Trigger to Vidicon circuits
Coincidence-anticoincidence circuit
Gating signal
Particle trajectory
PM tube
PM tube
PM tube
S
S
S
Counter
Counter
Counter
Target
LH_2
Strobe lamp
Lucite
window
Strobe lamp
Spark chamber
(one of several surrounding target)
Trigger amplifier
Pulse modulator
Strobe lamp supply
X Y
Vidicon camera
Core memory
Tape transport
Monitor kinescope

FIG. 2

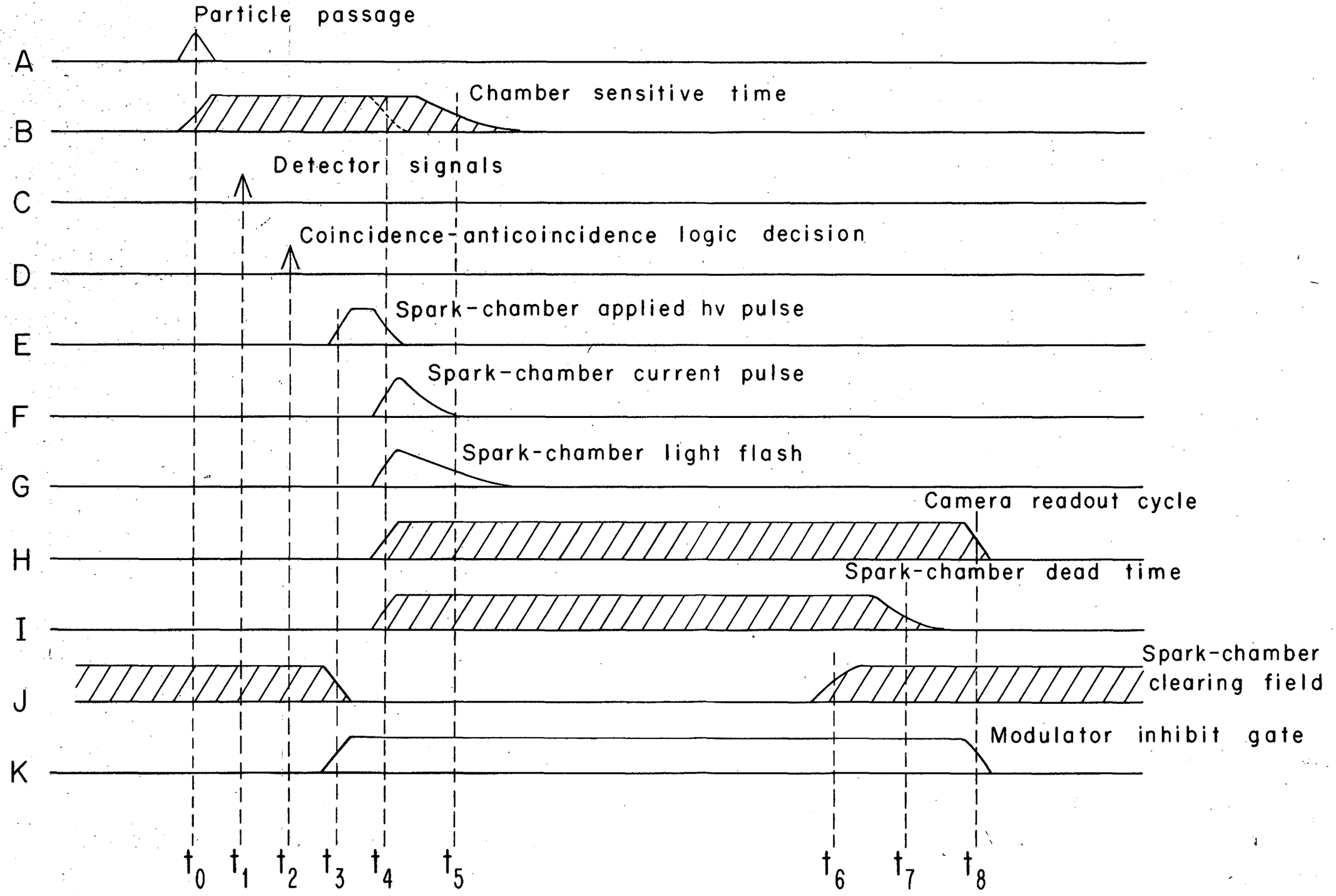
Particle passage
A
Chamber sensitive time
B
Detector signals
C
Coincidence-anticoincidence logic decision
D
Spark-chamber applied hv pulse
E
Spark-chamber current pulse
F
Spark-chamber light flash
G
Camera readout cycle
H
Spark-chamber dead time
I
Spark-chamber
clearing field
J
Modulator inhibit gate
K
t_0 t_1 t_2 t_3 t_4 t_5 t_6 t_7 t_8

FIG. 2

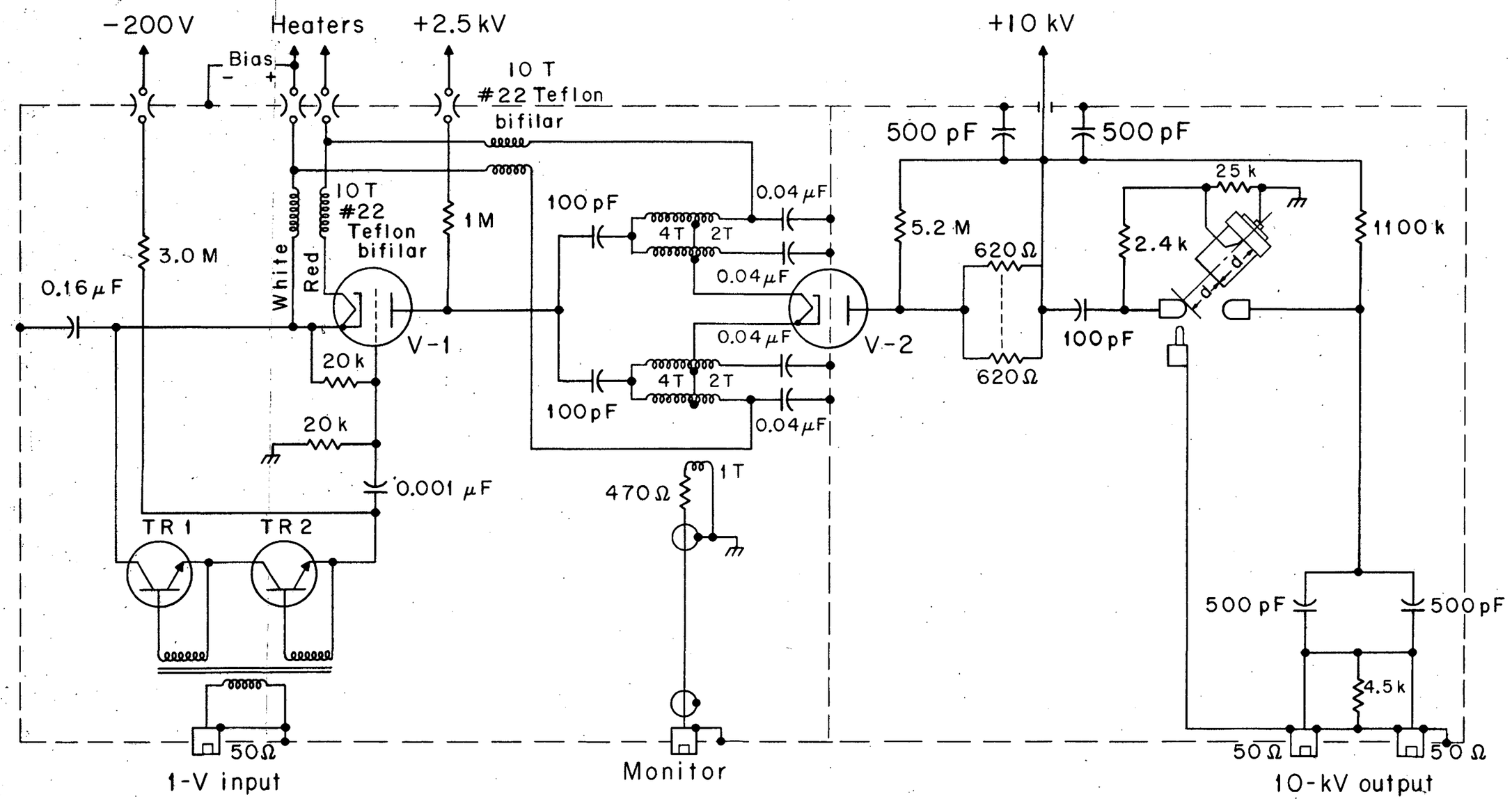
−200 V
Heaters
+2.5 kV
+10 kV
Bias
−
+
10 T
#22 Teflon
bifilar
3.0 M
0.16 μF
White
Red
10 T
#22
Teflon
bifilar
1 M
100 pF
0.04 μF
4T
2T
0.04 μF
V-1
V-2
20 k
20 k
0.001 μF
TR 1
TR 2
50 Ω
1-V input
100 pF
0.04 μF
4T
2T
0.04 μF
470 Ω
1T
Monitor
500 pF
500 pF
5.2 M
620 Ω
620 Ω
100 pF
25 k
2.4 k
1100 k
500 pF
500 pF
4.5 k
50 Ω
50 Ω
10-kV output

FIG 3

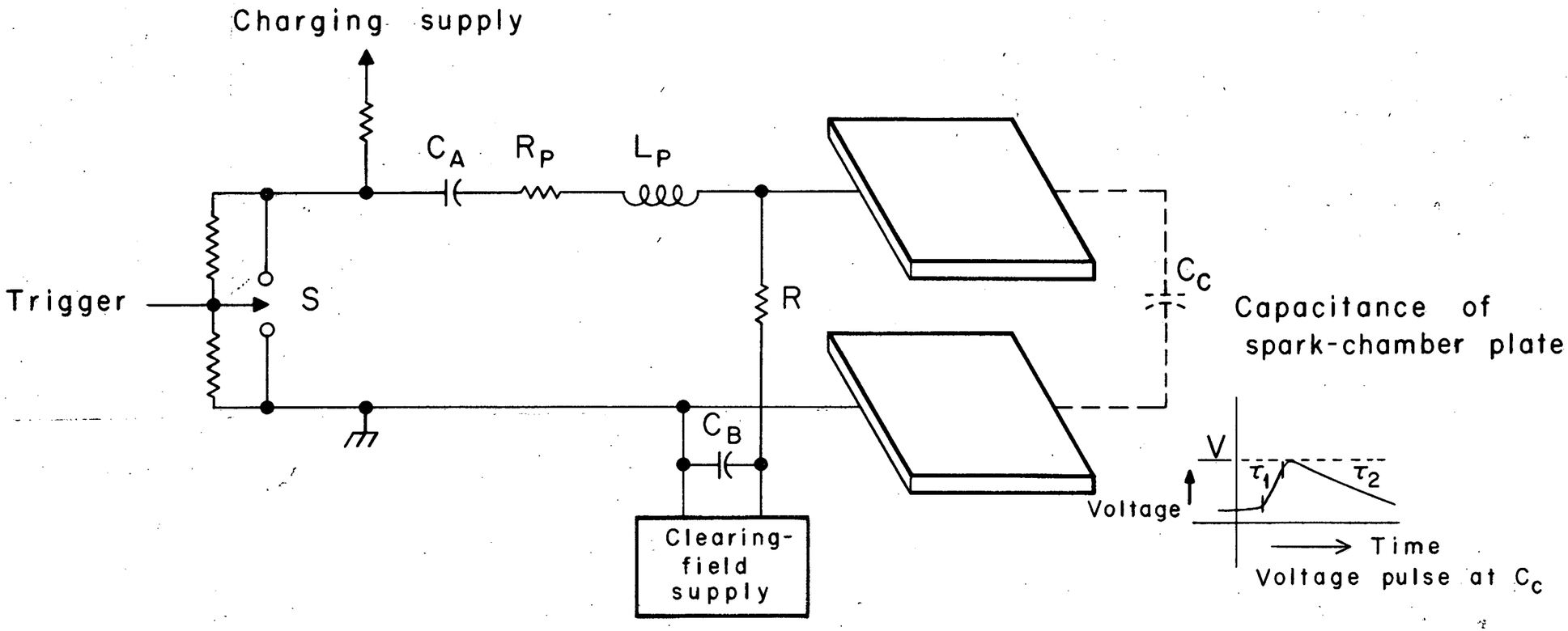
Charging supply
C_A
R_P
L_P
Trigger
S
R
C_C
Capacitance of spark-chamber plates
C_B
Clearing-field supply
V
τ_1
τ_2
Voltage
Time
Voltage pulse at C_c

Fig 4

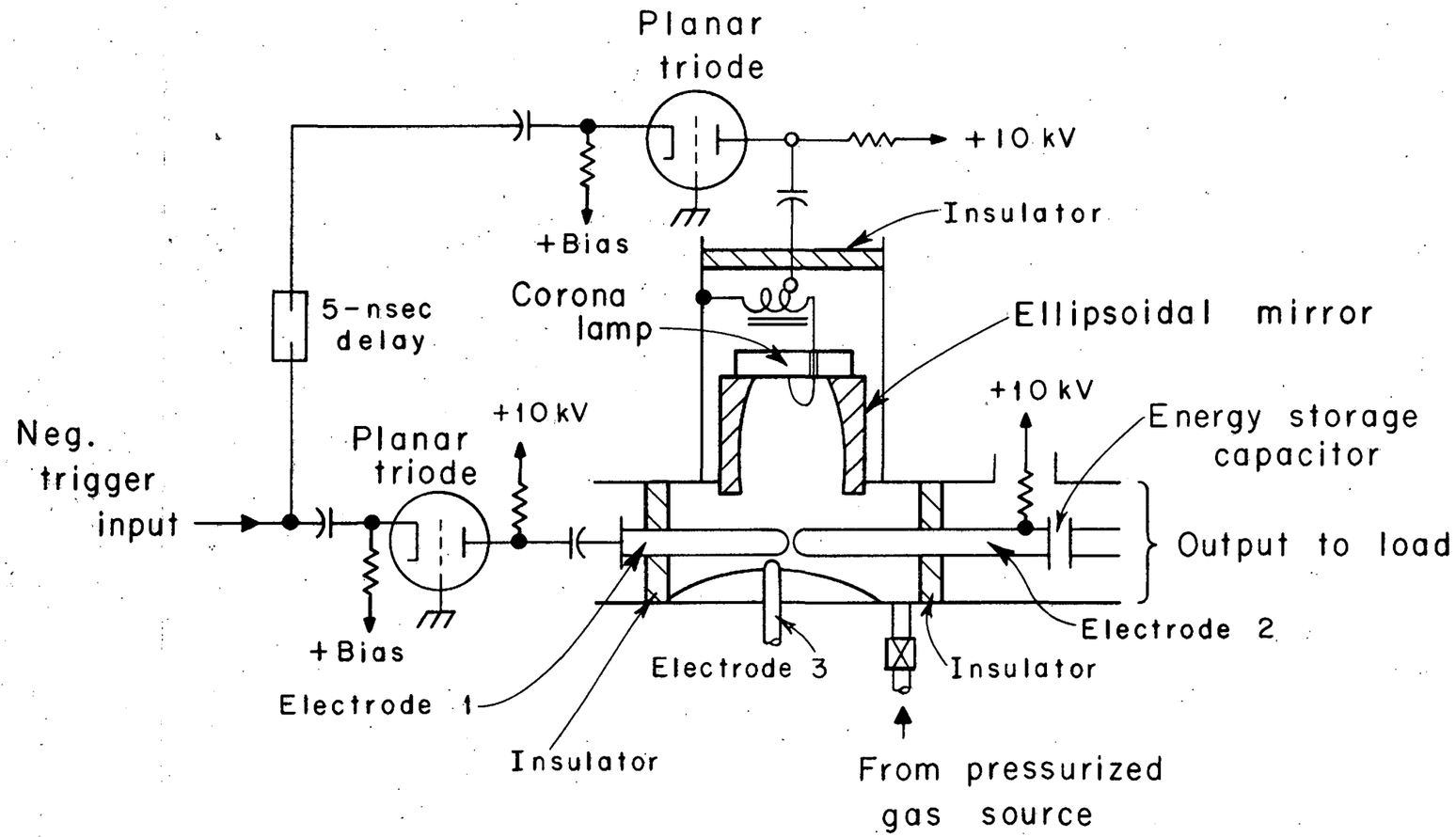
Planar
triode
+10 kV
Insulator
+Bias
Corona
lamp
5-nsec
delay
Ellipsoidal mirror
+10 kV
+10 kV
Energy storage
capacitor
Neg.
trigger
input
Planar
triode
Output to load
Electrode 2
+Bias
Electrode 3
Insulator
Electrode 1
Insulator
From pressurized
gas source

FIG 6

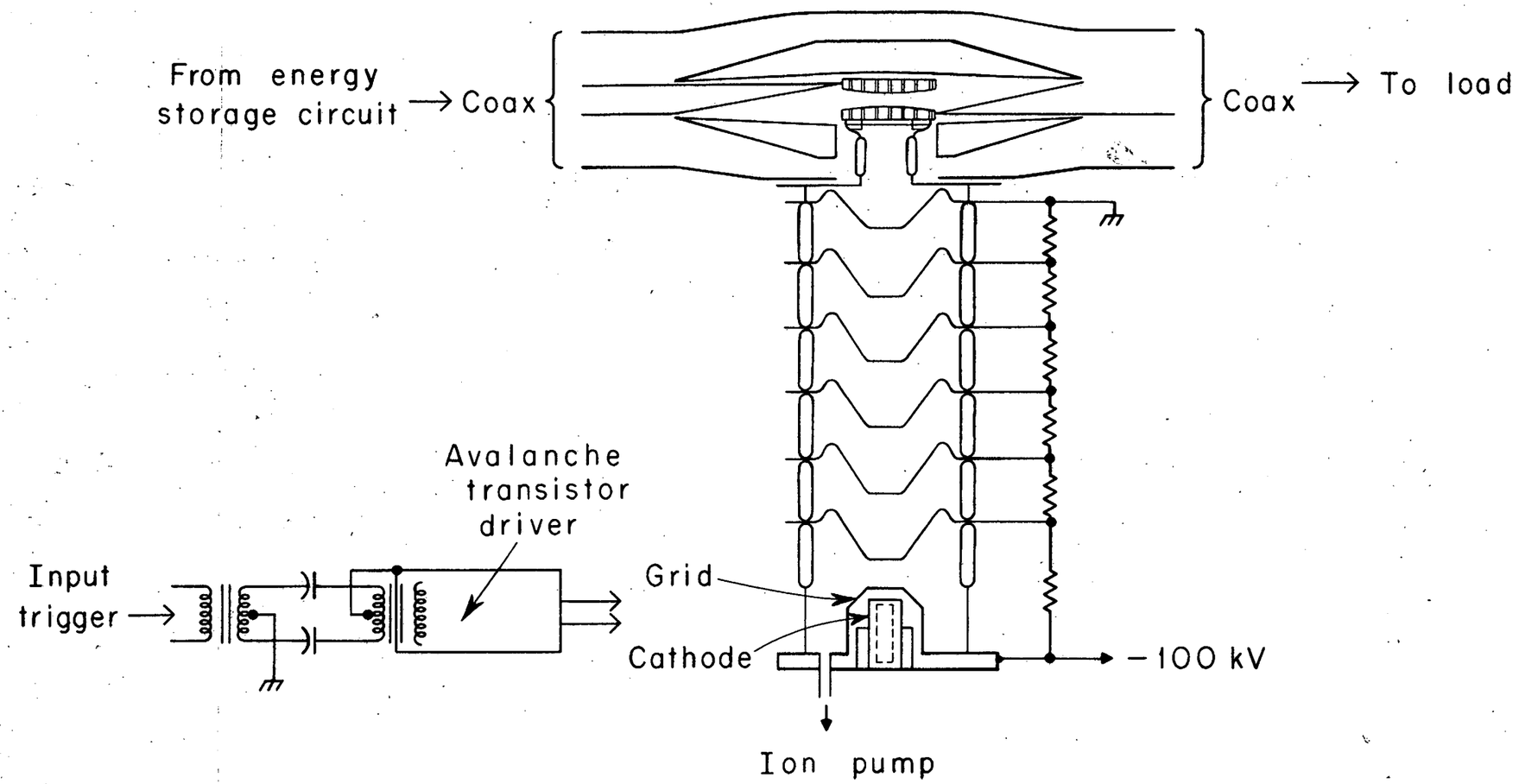
From energy storage circuit
Coax
Coax
To load
Avalanche transistor driver
Input trigger
Grid
Cathode
−100 kV
Ion pump

FIG. 1

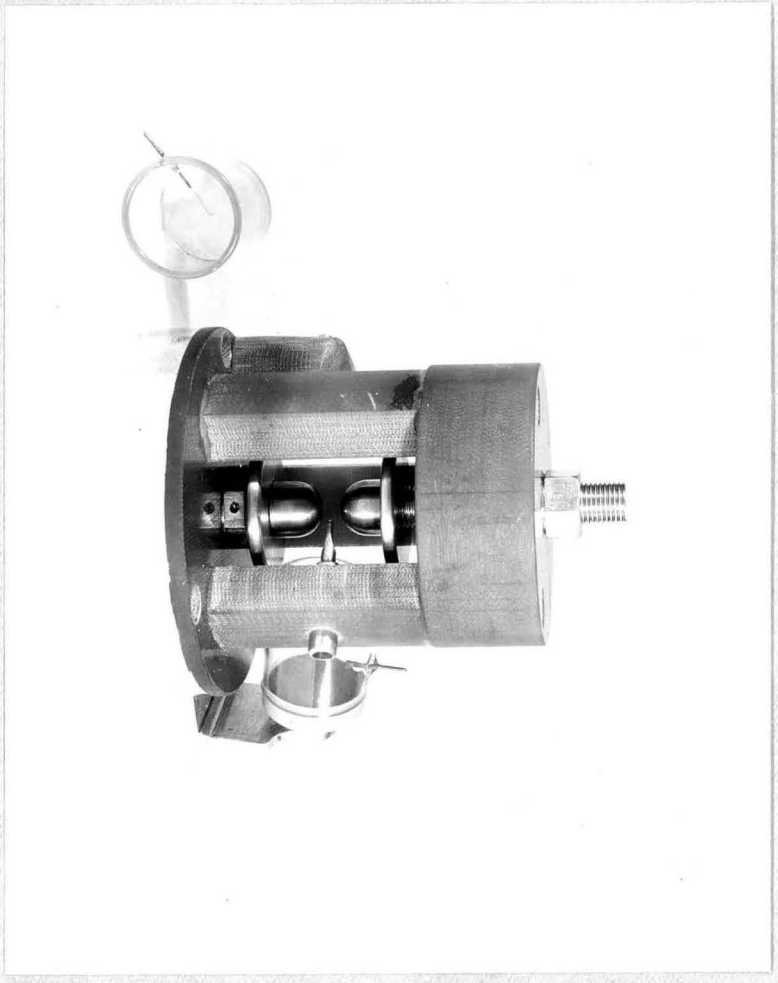

Fig. 5

6 Cut

8 Cut

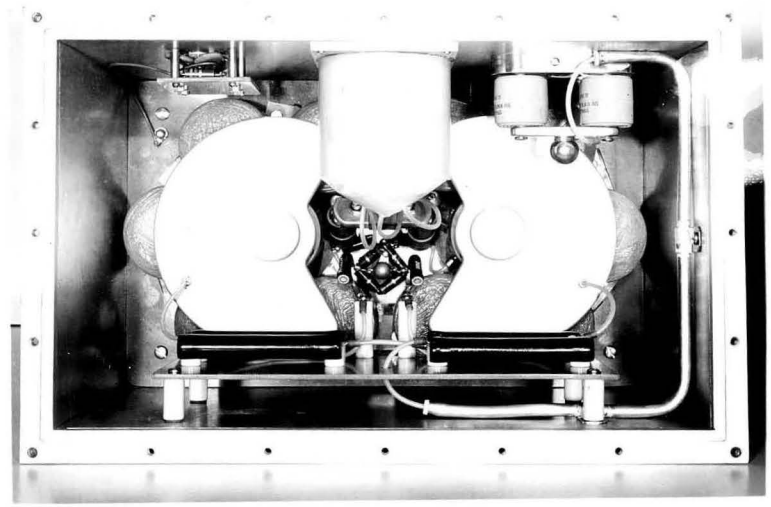

Fig. 11

Fig. 10